

# SIGNAL PROCESSING ENHANCEMENT OF AMPEROMETRIC BIOSENSORS FOR EMERGING BLOOD GLUCOSE MEASUREMENT/MONITORING

Maryamsadat SHOKREKHODAEI<sup>1</sup>, Stella QUINONES<sup>2</sup>,  
Ziba FAZEL<sup>3</sup>, Homer NAZERAN<sup>2</sup>

<sup>1</sup>Department of Electrical and Computer Engineering, The University of Texas at El Paso,  
500 W University Ave, TX 79968 El Paso, Texas, United States of America

<sup>2</sup>Department of Electrical and Computer Engineering, Faculty of Electrical and Computer Engineering,  
The University of Texas at El Paso, 500 W University Ave, TX 79968 El Paso, Texas, United States of America

<sup>3</sup>Department of Electrical Engineering, The Sharif University of Technology, Azadi Ave, Tehran, Iran

mshokrekhod@miners.utep.edu, stellaq@utep.edu, ziba\_fazel@ee.sharif.ir, hnazeran@utep.edu

DOI: 10.15598/aece.v17i1.3020

**Abstract.** In this paper, an overview of Amperometric Biosensors with application to chemical measurement systems is presented first. We then focus on signal processing enhancement of emerging Amperometric Biosensors suitable for eHealth applications by design and implementation of an analog four-path high-quality Band Pass Filter (BPF) with adjustable center frequency. This filter is placed prior to the ADC stage to remove the aliased noise and improve on the Signal-to-Noise Ratio (SNR). Finally, future trends in applying Amperometric Biosensors as user-friendly personalized glucose measurement devices are conceptualized and discussed.

## Keywords

*Amperometric, biosensor, diabetes, eHealth, glucose monitoring, signal processing.*

## 1. Introduction

A chemical sensor is a device that transduces (converts) chemical energy into an electrical signal. Chemical sensors consist of two parts: 1) a receptor that senses its input variations as a measurable form of energy and, 2) a transducer that converts the sensed energy into other quantities. The receptor's function is based on physical, chemical, or biochemical principles [1]. In a chemical-based sensor, the chemical reactions between the measurand and the receptor site increase the

output electrical signal. Similarly, in a biochemical-based sensor, the biochemical reactions at the receptor site serve as the source of the electrical signal [1]. These sensors are called "biosensors" for short.

Electrochemical sensors are the largest group of chemical sensors that convert chemical information into electrical signals. Their fast response, high sensitivity, and simplicity make them suitable for a variety of applications such as the diagnosis of disease, environmental monitoring, and food inspection, among others [2]. These sensors operate based on the enzymatic catalysis of a reaction that produces or consumes electrons [3]. Electrochemical sensors are divided into three main classes: 1) voltammetric, 2) potentiometric, and 3) conductometric [4]. Voltammetric sensors function according to the measurement of current-voltage variations. Amperometric Biosensors are a special case of these types of sensors. In Amperometric Biosensors, a fixed voltage applied to the electrode forces the chemical solution out of the equilibrium state. This results in reduction/oxidation (redox) reactions in the solution [5]. Consequently, a current signal is generated that flows through the electrode. The generated current signal has a known relationship to the concentration of the chemical substance in the solution.

In this paper, we highlight the conceptual design of an analog 4-path high quality (high Q) Band Pass Filter (BPF) with adjustable center frequency for improving the performance of emerging Glucose Amperometric Biosensors with potential applications to non-invasive personalized monitoring and eHealth.

The article is organized as follows. An overview of Amperometric Biosensors and a detailed description of their main building blocks are given in Sec. 2. and Sec. 3. , respectively. The details of the conceptual design and implementation of a high Q BPF as a means for enhancing the signal processing capabilities of the biosensor are presented in Sec. 4. Next, Sec. 5. focuses on our vision for the development of a user-friendly Amperometric glucose biosensor for monitoring and eHealth applications in the near future. Finally, Sec. 6. presents our conclusions.

## 2. Overview of Amperometric Biosensors

Figure 1 shows the block diagram for a conventional Amperometric Biosensor. It consists of an Electrode, a Control Logic block, a Potentiostat block, a Lock-in Amplifier (LIA), an Analog-to-Digital Converter (ADC), a Signal Processing block, and a Display Unit.

The Potentiostat block is comprised of two main sub-blocks: a Potential Control block and a Current Measurement (Readout) block [2]. The Potentiostat serves as an interface between the Electrode and the LIA. Electrochemical sensors use potentiostatic methods to detect changes in the dielectric properties of an electrode's surface.

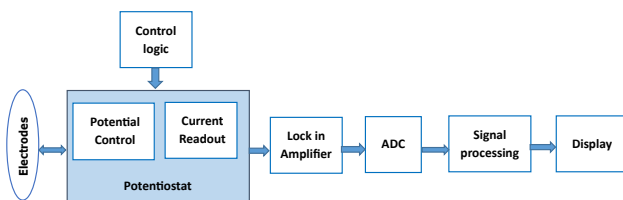


Fig. 1: Block diagram of a typical Amperometric Biosensor.

At the Electrode's (Electrochemical Cell's) surface, the chemical quantity of the analytes is sensed and converted into an electrical signal based on the reduction/oxidation (redox) reactions in the solution. The generated current signal is then measured by the Current Measurement block in the Potentiostat. Subsequently, a LIA is used to extract the weak signals and remove noise contamination. Next, the detected electrical signal is converted to digital form by the ADC. A Signal Processing unit then uses different algorithms to produce an output proportional to the chemical inputs based on the amplitude of the measured current signal. In the final stage, the acquired chemical information is displayed. The details of the building blocks of the Amperometric Biosensor are presented in the subsections below.

### 2.1. The Electrochemical Cell

The Electrochemical Cell is comprised of a two-electrode or a three-electrode structure. The former consists of a Working Electrode (WE), where electrochemical reactions take place, and a Reference Electrode (RE), which tracks the solution's electrical potential. In contrast, a three-electrode structure with one more electrode, named the Counter or Auxiliary Electrode (CE), offers better performance. The CE supplies the current required for the electrochemical reactions at the WE in order to maintain the stability of the RE [2]. As such, the three-electrode structure is preferable. The voltage difference between the WE and RE should be kept constant so that the current through the RE will ideally be zero.

One of the simplest equivalent electrical circuit models for the Electrochemical Cell is the Randles Model shown in Fig. 2. This model is comprised of a double-layer capacitance (denoted by  $C_{REF}$ ), in parallel with a polarization resistance (represented as  $R_{REF}$ ), which is also described as a charge transfer resistance, and the solution resistance symbolized by  $RAUX$  [3] and [4].

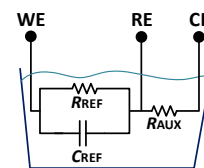


Fig. 2: Randles model for electrochemical cells.

### 2.2. The Potentiostat

The Potentiostat is comprised of a Potential Control Block and a Current Measurement/Readout block. Figure 3 shows the Potential Control block with three electrodes in which the WE is connected to the ground. The potential difference between the WE and RE ( $V_{cell}$ ) is kept at a certain potential value ( $V_{in}$ ) by sinking or sourcing currents from or into the sensor through the CE, which measures the current [3].

In the Current Measurement block, the current flowing through the CE is sensed by inserting a resistor into the feedback loop of the Potential Control block (Fig. 3) and the Instrumentation Amplifier (IA) is used to measure the voltage difference across this resistor [3]. In this case, the WE is grounded. There is another approach for measuring the current through the WE. It is achieved by using a Trans-Impedance Amplifier (TIA). In this case, the WE is virtually grounded.

Based on the first approach mentioned above, we can design the IA so that its output voltage has minimal dependency on the thermal noise of the resistors used

in its circuit [3] and it offers better performance in comparison to the virtually grounded case (TIA) in which environmental noise easily affects output [6]. Additionally, the IA with a wider output swing and a more effective rejection of second-order harmonics produces better linearity.

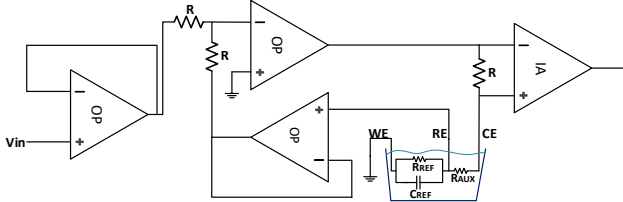


Fig. 3: The potential control and current measurement blocks [3].

### 3. The Lock-In Amplifier

The Lock-In Amplifier (LIA) uses a phase sensitive detection method to extract weak AC signals at a specific reference frequency and phase from an extremely noisy environment. The LIA improves the Signal-to-Noise Ratio (SNR) due to its ability to cancel out undesirable harmonics and interferences [7].

#### 3.1. The LIA Structure and Its Theoretical Framework

Figure 4 shows the structure/essential components of a LIA using a down-converted mixer followed by an adjustable low pass filter. After being split, each component of the input signal is separately multiplied by the reference signal and its 90° phase-shifted replica [7] and [8]. The Oscillator signal applied to the Mixer is either a sine wave or a square wave.

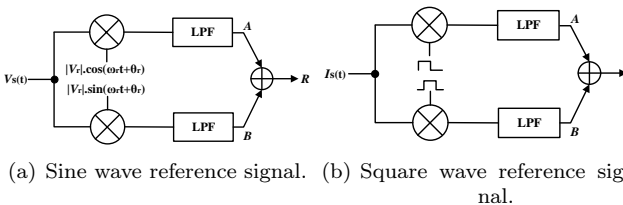


Fig. 4: Block diagram of the Lock-in Amplifier.

In Fig. 4(a), the converted signal (in the frequency domain) in path A preceding the LPF is defined as in Eq. (1).

$$V_A(\omega) = V_s(\omega - \omega_r) \cdot |V_r| \cdot \frac{e^{j\theta_r}}{2} + V_s(\omega + \omega_r) \cdot |V_r| \cdot \frac{e^{-j\theta_r}}{2}, \quad (1)$$

where  $V_s(\omega)$  is Fourier transform of the input signal and  $|V_r|$ ,  $\omega_r$  and  $\theta_r$  are the amplitude, frequency, and phase, respectively, of the reference signal applied to the Mixer. We define  $\omega_s$  and  $\theta_s$  as frequency and phase of the input signal  $V_s(t)$  to rewrite  $V_A(\omega)$  as Eq. (2).

$$V_A(\omega) = |V_s(-\omega_s + \omega_r)| \cdot e^{-j\theta_s} |V_r| \cdot \frac{e^{j\theta_r}}{2} + |V_s(+\omega_s + \omega_r)| \cdot e^{j\theta_s} |V_r| \cdot \frac{e^{j\theta_r}}{2} + |V_s(-\omega_s - \omega_r)| \cdot e^{-j\theta_s} |V_r| \cdot \frac{e^{-j\theta_r}}{2} + |V_s(\omega_s - \omega_r)| \cdot e^{j\theta_s} |V_r| \cdot \frac{e^{-j\theta_r}}{2}. \quad (2)$$

In order to extract the amplitude of the desired voltage signal, a low pass filter is used to remove the high-frequency component at  $\omega_s + \omega_r$ . Based on Eq. (2), for  $\omega_s = \omega_r$ , the filtered output in the frequency domain is given as follows:

$$V_A(\omega) = |V_r| \cdot |V_s| \cdot e^{-j\theta_s} \cdot \frac{e^{j\theta_r}}{2} + |V_r| \cdot |V_s| \cdot e^{j\theta_s} \cdot \frac{e^{-j\theta_r}}{2} = |V_r| \cdot |V_s| \cdot \cos(\theta_r - \theta_s). \quad (3)$$

As indicated in Eq. (3), the voltage signal in path A depends on the phase difference ( $\theta$ ) between the input signal and reference signals.  $V_A(\omega)$  has its maximum value at  $\theta = 0^\circ$  and its minimum value at  $\theta = 90^\circ$ . To eliminate the phase dependency, the second path B is used to multiply the signal  $V_s$  with a 90° shifted reference signal. The low pass filtered output B is given by Eq. (4) for the condition where  $\omega_s = \omega_r$ .

$$V_B(\omega) = |V_r| \cdot |V_s| \cdot e^{-j\theta_s} \cdot \frac{e^{j\theta_r}}{2j} - |V_r| \cdot |V_s| \cdot e^{j\theta_s} \cdot \frac{e^{-j\theta_r}}{2j} = |V_r| \cdot |V_s| \cdot \sin(\theta_r - \theta_s). \quad (4)$$

The outputs of the Mixers passing through the Low Pass Filters result in the two output voltages  $V_A(t)$  and  $V_B(t)$ . The total amplitude  $R$  and the phase  $\theta$  are easily derived from  $V_A(t)$  and  $V_B(t)$  by transforming the Cartesian coordinates into polar coordinates based on Eq. (5). We can infer that the phase dependency of the filtered signal is removed by this quadratic structure.

$$R = \sqrt{V_A^2(t) + V_B^2(t)}, \quad \theta = \arctan\left(\frac{V_B(t)}{V_A(t)}\right). \quad (5)$$

The LIA detects the DC component of the desired signal and rejects noise. The attenuation of unwanted

harmonic components depends on the LPF bandwidth. A narrower LPF bandwidth results in a better noise rejection closer to the reference frequency. However, the amount of time needed for the filter output to settle at its new value will be increased. Thus, there is a trade-off between higher SNRs and time resolution.

The theoretical discussion of the LIA presented here assumes a sine wave for the reference signal. However, some LIAs use a square wave as the reference signal. We recall, that in the frequency domain, a sine wave represented by two harmonic tones at the reference frequency produces a pure measurement at the fundamental frequency. In contrast, a square wave represented by harmonic tones at the reference frequency produces all of the odd harmonics of the signal. Figure 4(b) shows the LIA with a square wave reference signal and a current input signal  $I_s(t)$ . The converted current signal in Path A, preceding the LPF, is then defined by Eq. (6) in both time and frequency domains based on the Fourier analysis of a square wave as follows:

$$\begin{aligned}
 I_A(t) &= I_s(t) \cdot \sum_{n=-\infty}^{n=+\infty} |V_r| \cdot \\
 &\cdot \frac{\sin(\frac{n\pi}{2})}{n\pi} \cdot e^{-jn\omega_r(\frac{T_r}{4})} \cdot e^{jn\omega_r t}, \\
 I_A(\omega) &= I_s(t) * \sum_{n=-\infty}^{n=+\infty} |V_r| \cdot \\
 &\cdot \frac{\sin(\frac{n\pi}{2})}{n\pi} \cdot e^{-jn\omega_r(\frac{T_r}{4})} \cdot \delta(\omega - n\omega_r), \\
 I_A(\omega) &= \sum_{n=-\infty}^{n=+\infty} |V_r| \cdot \\
 &\cdot \frac{\sin(\frac{n\pi}{2})}{n\pi} \cdot e^{-jn(\frac{\pi}{2})} \cdot I_s(\omega - n\omega_r),
 \end{aligned} \tag{6}$$

where  $|V_r|$  and  $\omega_r$  are amplitude and frequency of the reference signal applied to the mixer and \* symbolizes the convolution operation.

Based on the definition of  $I_A(\omega)$ , if  $\omega_s = \omega_r$ , the desired signal in path A is converted to a DC signal (frequency = 0) with a current gain of  $(1/\pi)$  for  $n = 1$ . However, there will be unwanted harmonic frequencies for odd values of n resulting in more interference and noise. Another problem is noise folding onto the desired signal. For example, the unwanted component at  $3\omega_s$  will be folded back into the band of interest (at DC) for  $n = 3$ , thereby disrupting the desired signal.

### 3.2. The Digital LIA vs Analog LIA

In the section above, the LIA concept was presented in the analog domain. We could likewise discuss this concept in the digital domain and implement it by using a Digital Signal Processing (DSP) chip or a Field Programmable Gate Array (FPGA). Reference [9] de-

tails the analog implementation of the LIA with phase alignment through feedback control; and Ref. [10] proposes a digital algorithm for the implementation of the LIA using a square wave reference signal. They implemented this algorithm through additions and subtractions to speed up the computations in the LIA. Reference [11] proposes a semi-digital phase tuning loop to increase the LIA’s sensitivity by measuring the phase difference between the input and reference signals and then adjusting the phase.

Tab. 1: Comparison between analog/digital LIAs.

	Digital LIA	Analog LIA
Much less prone to mismatch between I and Q path	x	
Much less prone to the output Offset	x	
Much less prone to the gain error due to reference amplitude drift	x	
Much less prone to temperature changes	x	
No limitation in dynamic range due to nonlinearity of mixer	x	
Multiple demodulators & analyzing a signal at multiple different frequencies without loss of SNR	x	
Good choice when there is limited computing power for mathematical operation		x

Table 1 shows the comparison between the Digital and Analog LIAs. Digital technology can overcome any mismatch between the in-phase and quadrature (I/Q) signal paths. This I/Q amplitude and phase mismatch causes sideband and unwanted frequency harmonics, thereby limiting the measurement accuracy [8]. Moreover, the output offset in the analog LIA contributes to the DC error and zero drift. We can solve the offset problem by using a digital multiplier. Gain error due to the amplitude drift in the reference signal is another problem, which is a common issue in analog LIAs, while a digital reference signal is without any amplitude changes [12]. Additionally, analog LIAs suffer from measurement errors due to temperature changes. The dynamic range (the ratio of the maximum tolerable noise to the minimum desired signal that can be detected by a system) of analog LIAs is limited by the nonlinearity of their Mixer/Filter and a nonlinear operation results in poor noise rejection. In contrast, the dynamic range of a digital LIA is only limited by the resolution, linearity, accuracy, and aliasing in the ADC. Additionally, a Digital Processor has high calculation power and can perform different analyses without loss of the SNR [8]. Considering all of the above-mentioned factors and Tab. 1, we can easily observe that the digital LIAs offer superior performance compared to analog LIAs. In situations where digital LIAs using complex

mathematical algorithms consume a large amount of power, analog LIAs may offer a better choice, especially when computing power is limited.

## 4. Signal Processing Enhancement

Figure 5 shows the block diagram of a proposed design to enhance the signal processing capability of the Amperometric sensor using the three-electrode structure. As was discussed in Sec. 2, the three-electrode sensor topology offers superior performance compared to the two-electrode version because the CE keeps the RE voltage constant by providing the current required for the electrochemical reaction at the WE electrode. The  $V_{cell}$  is applied by the Potential Control block while the WE electrode is connected to ground. When the WE is connected to real instead of virtual ground, the sensor is less prone to noise. The implementation of the Current Measurement block through the use of the Instrumentation Amplifier (with differential inputs) has the ability to reject any existing second-order harmonic distortions and common mode signals. Ultimately the aforementioned design is preferable for implementation compared to the one that implements the TIA through the WE. The Potential Control and Current Measurement/Readout blocks could be implemented by using CMOS technology. A system-on-chip approach results in a smaller size for the electrodes and is capable of lower current detection.

Based on the discussion presented in section III and the factors listed in Tab. 1, we can conclude that the digital implementation of the LIA results in a better performance compared to that achieved by the analog LIA in terms of mismatch, output offset, gain error, linearity, stability, and sensitivity to temperature changes. The digital LIA can be readily determined by using FPGAs. These devices can be flexibly programmed to carry out almost any desired signal processing task in real time and produce any kind of information about the Chemical Cell by doing sophisticated analysis on the desired discrete voltage signal.

Converting the sensed analog signal to its digital form requires an ADC in front of the digital LIA. Adding a high Q BPF between the Potentiostat and the ADC can reduce the aliasing limitation in the ADC due to high-frequency noise. Undesired harmonic rejection prior to the ADC can relax the requirements for a high sampling rate. This reduction in the sampling rate, in turn, can lower the power consumption requirements. As a result, there is no need to be concerned about the utilization of complex techniques [13] to obtain an ADC with both high sampling rate and low power consumption. Furthermore, there is no need to implement

complex algorithms in the digital domain to clean the sensed signals from the high amount of noise before the ADC. This feature in itself reduces the volume of the required digital computations. In the proposed design, a 4-path BPF with adjustable center frequency is inserted in front of the ADC. This filter is designed by using passive switches and capacitors and is in high demand especially over high-frequency bands where the implementation of a BPF with a high Q is challenging. The 4-path BPF with a high Q introduces negligible power, noise, and non-linearity to the main circuit [14] and [15]. The current mode passive Mixers draw no DC current, so flicker noise is negligible in a well-designed mixer. Current mode passive Mixers are more linear than their active counterparts [16].

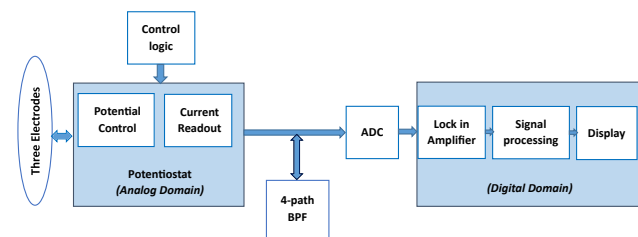


Fig. 5: Signal processing enhancement of the Amperometric sensor.

### 4.1. Conceptual Design and Simulation Results of 4-Path Band Pass Filter

Figure 6 shows the proposed 4-path BPF including 4 Mixers (switches) and 4 capacitors. The time-shift between the two successive paths is equal to  $T/N$ , where  $T$  is the period of the Mixer clock and  $N$  is the number of paths. The phase shift between the two successive paths in the 4-path BPF is  $90^\circ$  and mixer clock has duty cycle of 25 % [15].

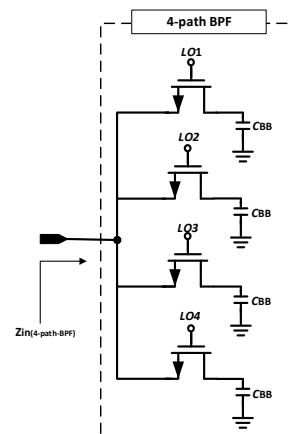


Fig. 6: The schematic of the 4-path BPF with high quality (Q) factor.

Equation (7) shows the input impedance of the 4-path BPF [14].

$$Z_{in_{4path\_BPF}}(\omega) = R_{sw} + 4 \cdot \sum_{n=-\infty}^{n=+\infty} Z_{BB}(\omega - n\omega_{LO}) \cdot |an|^2, \quad (7)$$

$$|an| = \frac{\sin(\frac{n\pi}{N})}{n\pi},$$

where  $R_{sw}$  is the switch resistor,  $Z_{BB}$  is the capacitor's impedance  $1/(jC_{BB}\omega)$ ,  $N$  is the number of paths, and  $\omega_{LO}$  is the mixing frequency. The input impedance is significantly small except at frequencies close to  $\omega_{LO}$  and its integer multiples; the input impedance also decreases in increments of  $n$ . As the input impedance around  $\omega_{LO}$  is of main interest, Eq. (7) is simplified to Eq. (8) for  $n = \pm 1$  [14] as follows:

$$Z_{in_{4path\_BPF}}(\omega) \approx R_{sw} + \left(\frac{2}{\pi^2}\right) \cdot [Z_{BB}(\omega - \omega_{LO}) + Z_{BB}(\omega + \omega_{LO})] \approx R_{sw} + \left(\frac{2}{\pi^2}\right) \cdot \left[\frac{1}{jC_{BB}(\omega - \omega_{LO})} + \frac{1}{jC_{BB}(\omega + \omega_{LO})}\right]. \quad (8)$$

Based on Eq. (8), the input impedance of the 4-path BPF is ideally infinite for the desired signal and is much less for undesired inputs. Figure 7 shows the input impedance ( $Z_{in_{4-pathBPF}}$ ) of the designed circuit with an arbitrary mixing frequency of 10 kHz and a  $C_{BB} = 30 \mu\text{F}$ . The input impedance has a BPF behaviour near the center frequency, which is determined by the mixing clock frequency ( $\omega_{LO}$ ). Therefore,

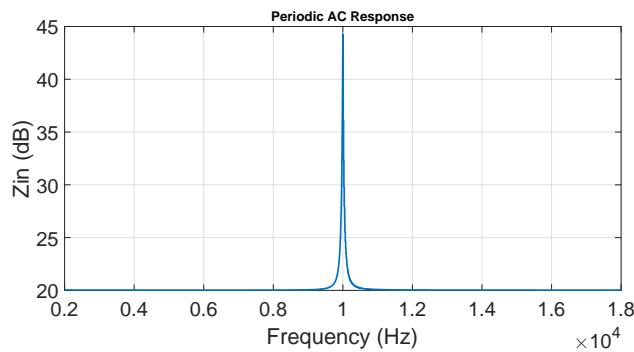


Fig. 7: Input Impedance of designed 4-path BPF.

the clock frequency, which is applied to the switches, should be equal to the frequency of the desired input signal. The input impedance of the 4-path BPF is 44 dB for the desired signal at 10 kHz and is 24 dB lower for the undesired input signal close to 10 kHz (about 1/16 of the maximum impedance). Consequently, the undesired current signal will be filtered out by the 4-path BPF and will not enter the next block (ADC). In other words, the unwanted signal sinks into

the BPF as the input impedance of this filter is much lower for the unwanted signal. However, the desired signal is subjected to the opposite effect; that is, the desired current signal sees very high impedance at the input of the BPF and will pass unattenuated to the next block (ADC) without any current sinking in to the 4-path BPF.

The Noise Figure (NF) of the designed circuit is 3.8 dB at the desired frequency as shown in Fig. 8. This value is negligible considering its significant positive impact on improving the signal quality by achieving a 24 dB rejection of the undesired signal. Moreover, the total NF of the Amperometric Sensor has less dependency on the NF of the last stage, thereby alleviating any design concerns about the NF of the BPF.

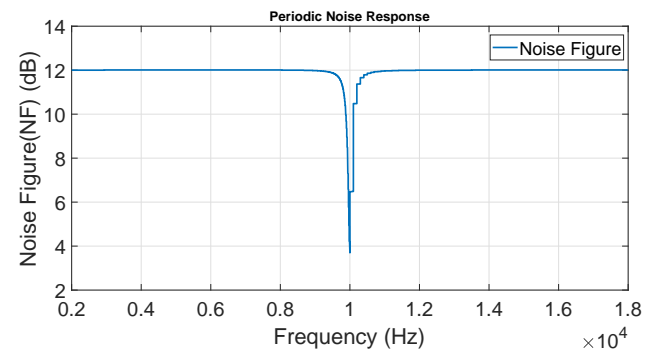


Fig. 8: Noise Figure of the designed 4-path BPF.

## 4.2. Experimental Results

The circuit schematic of 4-path BPF in Fig. 9(a) is implemented by using discrete ICs connected on a bread board (see Fig. 9(b)). MOSFETs are switched by clock frequency of 10 kHz and duty cycle of 25%. Phase shift of 90° is between two successive clock signals. MOSFETs operate as switches in cut off and triode regions.

Figure 10(a), Fig. 10(b) and Fig. 10(c) represent voltage signal measured at node Y when the 100 mV input signal is applied with frequency of 9.9 kHz, 10 kHz and 10.1 kHz respectively. In a case that input signal has the frequency of 10 kHz (equal with the clock frequency), there is no obvious change in the amplitude of measured signal at node Y. However, there is 86.6% reduction in the amplitude of measured signal when 100 mV input signal applied with the frequency of 10.1 kHz and 9.9 kHz (around the clock frequency).

Figure 11(a) and Fig. 11(b) show the frequency spectrum of signal at node Y when the input signal has the frequency of 10 kHz and 10.1 kHz respectively. The amplitude of the first harmonic at 10 kHz (Fig. 11(a)) is 17.5 dB more than the first harmonic at 10.1 kHz (Fig. 11(b)). According to measurement results, unwanted input signals with frequency less than 9.9 kHz and more than 10.1 kHz are rejected (17.5 dB)

by implemented 4-path BPF with center frequency of 10 kHz.

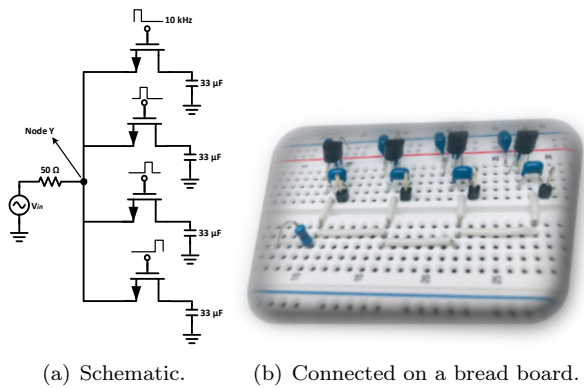
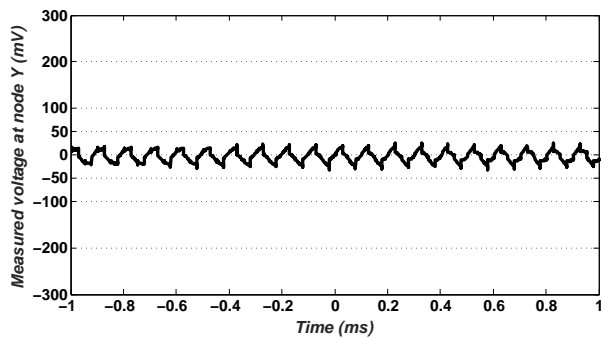
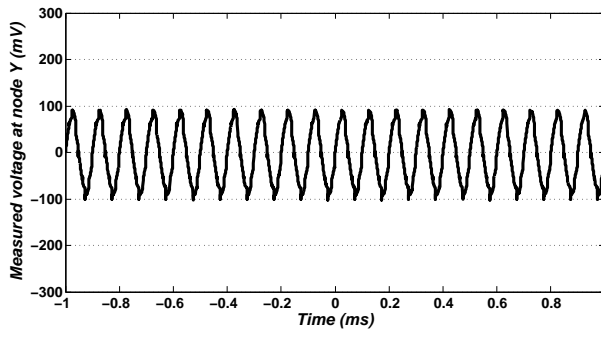


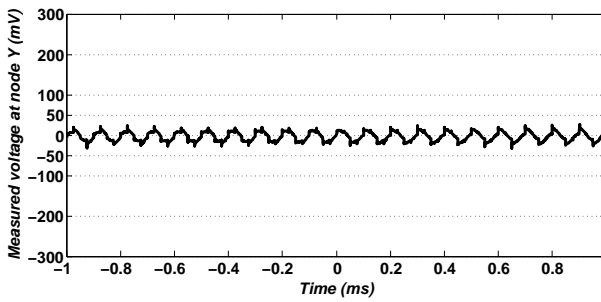
Fig. 9: Implemented circuit.



(a) 9.9 kHz.

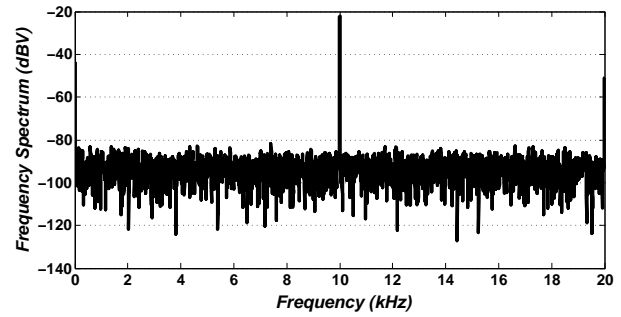


(b) 10 kHz.

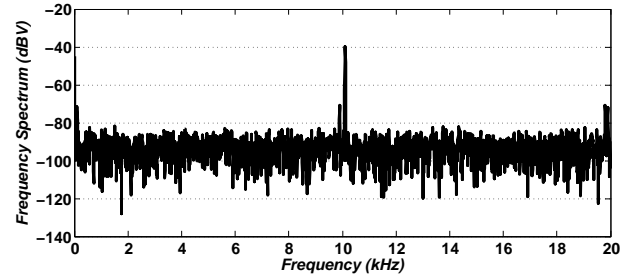


(c) 10.1 kHz.

Fig. 10: Measured voltage signal at node Y when the input signal has the frequency of.



(a) 10 kHz.



(b) 10.1 kHz.

Fig. 11: Frequency spectrum of signal at node Y.

## 5. Tissue Integrated Amperometric Biosensor for Glucose Measurement

As mentioned above, electrochemical biosensors use potentiostatic methods for detecting changes in the dielectric properties of their electrode surface. These biosensors have the ability to respond to antigens, antibodies, proteins, and metal ions [3]. Electrochemical biosensors can also be used for glucose measurement systems. Blood glucose concentration monitoring is required for effective glycemic control in persons with diabetes. One of the most common methods of daily glucose measurement/monitoring is the finger prick or finger sticking method, which involves placing a drop of blood on a chemically-active disposable test-strip and measuring the sugar concentration in it. This method is inconvenient for many people with diabetes. Consequently, there is a great need for a “needleless” user-friendly continuous blood glucose measurement/monitoring approach. Because the Amperometric Biosensor for glucose measurement is primarily based on the activity of the glucose oxidase enzyme at the surface of various electrodes, this leads to the production of gluconic acid and hydrogen peroxide [17] and [18]. By adding one more step to the implementation of the Amperometric Biosensor into human tissue, we can envision the further development of a non-invasive glucose measurement/monitoring biosensor targeting a variety of applications including eHealth. Figure 12

shows the block diagram of our proposed glucose biosensor. This vision would facilitate and guide the development and realization of emerging non-invasive continuous blood glucose sensing/monitoring in persons with diabetes.

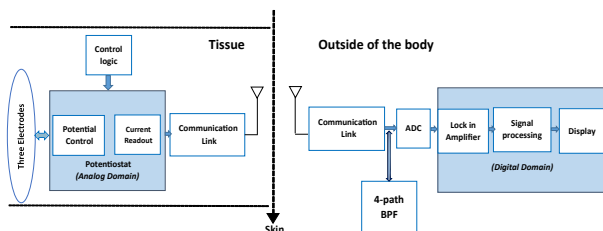


Fig. 12: Tissue integrated Amperometric.

There are two methods for measuring glucose levels in the blood: 1) the first, based on the enzymatic reactions catalyzed by glucose oxidase, uses an oxygen sensor to measure the change of oxygen concentration, which bears a known relationship with the blood glucose concentration; and 2) the second is based on the fact that the dielectric constant of blood increases as the glucose concentration in the solution decreases [19].

Because the former method involves enzyme immobilization techniques as well as a proper enzymatic biosensor design, it presents considerable challenges. A way forward to resolve these difficulties is to explore the use of the dielectric constant of blood glucose to measure the voltage applied to the electrode at an optimal frequency. In other words, as the dielectric constant of the blood is dependent upon glucose levels, the estimated value of the corresponding circuit element (at the optimal frequency) in the equivalent electrical circuit model of the electrochemical cell may provide a sensitive indicator of glucose levels. Of course, special attention must be paid to selecting the frequency of the voltage applied to the electrode so that blood conductivity is more sensitively related to the glucose concentration. In addition, there are other factors that must be carefully considered such as the life span of the implanted sensor, the foreign body reaction of the blood in response to an implanted device (blood tissue bio-compatibility issues), as well as the sensor's small size and low power consumption.

Currently, there are a number of possible methods for non-invasive, wearable, continuous blood glucose monitoring/measurement including light scattering [20], the transmission/reflection of optical waves at specific wavelengths, and so on [21]. However, the most challenging aspect of such approaches is that the measurement results are dependent not only on the glucose concentration but also on different components of the blood, temperature, skin moisture and thickness as well as other physiological factors such as age and skin color.

## 6. Conclusions

In this paper, we gave an overview of Amperometric Biosensors by presenting a detailed description of their building blocks as well as a comparison of different approaches for their design. We paid special attention to the conceptual design and implementation of an analog 4-path high Q BPF with adjustable center frequency, inserted between the Potentiostat and the ADC, to reject unwanted harmonics and improve the SNR. This design offers the advantage of improving the anti-aliasing part of the ADC, which in turn results in a high-quality digital signal at its output. The 4-path high Q BPF with adjustable center frequency is designed by using passive switches and capacitors that have low noise and power consumption. We also proposed one possible approach for the development of non-invasive glucose measurement/monitoring by leveraging a tissue-integrated Amperometric glucose sensor. This sensor offers the potential to track blood glucose variations reliably based on changes in the dielectric constant of blood glucose. We expect that our approach will improve the performance of emerging Glucose Amperometric Biosensors with applications to non-invasive personalized monitoring and eHealth.

## References

- [1] HULANICKI, A., S. GEAB and F. INGMAN. Chemical sensors: definitions and classification. *Pure and Applied Chemistry*. 1991, vol. 63, iss. 9, pp. 1247–1250. ISSN 0033-4545. DOI: 10.1351/pac199163091247.
- [2] WANG, W. S., H. Y. HUANG, S. C. CHEN, K. C. HO, C. Y. LIN, T. C. CHOU, C. H. HU, W. F. WANG, C. F. WU and C. H. LUO. Real-Time Telemetry System for Amperometric and Potentiometric Electrochemical Sensors. *Sensors*. 2011, vol. 11, iss. 9, pp. 8593–8610. ISSN 1424-8220. DOI: 10.3390/s110908593.
- [3] VILLAGRASA, J. P., J. COLOMER-FARRARONS and P. L. MIRIBEL. *Bioelectronics for Amperometric Biosensors. State of the Art in Biosensors Toonika Rincken* [online]. IntechOpen, 2013. pp. 241–247. DOI: 10.5772/52248.
- [4] COLOMER-FARRARONS, J., P. LI MIRIBEL-CATALA, A. I. RODRIGUEZ-VILLAREAL and J. SAMITIER. *Portable Bio-Devices: Design of electrochemical instruments from miniaturized to implantable devices* [online]. IntechOpen, 2011. pp. 374–400. DOI: 10.5772/17212.
- [5] NIC, M., J. JIRAT and B. COSATA *Compendium of Chemical Terminology*. 1st ed. Cambridge: In-

- ternational Union of Pure and Applied Chemistry, 2006.
- [6] WANG, W.-S., W.-T. KUO, H.-Y. HUANG and C.-H. LUO. A Wide Dynamic Range CMOS Potentiostat for Amperometric Chemical Sensor. *Sensors*. 2010, vol. 10, iss. 3, pp. 1782–1797. ISSN 1424-8220. DOI: 10.3390/s100301782.
- [7] SHOKREKHODAEI, M., S. QUINONES, R. MARTINEK and H. NAZERAN. A Robust PPG-based Heart Rate Monitor for Fitness and eHealth Applications. In: *2018 IEEE 20th International Conference on e-Health Networking, Applications and Services (Healthcom)*. Ostrava: IEEE, 2018, pp. 1–5. ISBN 978-1-5386-4294-8. DOI: 10.1109/HealthCom.2018.8531082.
- [8] Principles of Lock-in Detection and the State of the Art. In: *Zurich Instruments* [online]. 2016. Available at: [https://www.zhinst.com/sites/default/files/li\\_primer/zi\\_whitepaper\\_principles\\_of\\_lock-in\\_detection.pdf](https://www.zhinst.com/sites/default/files/li_primer/zi_whitepaper_principles_of_lock-in_detection.pdf).
- [9] DE MARCELLIS, A., G. FERRI, A. D'AMICO, C. DI NATALE and E. MARTINELLI. A Fully-Analog Lock-In Amplifier With Automatic Phase Alignment for Accurate Measurements of ppb Gas Concentrations. *IEEE Sensors Journal*. 2012, vol. 12, iss. 5, pp. 1377–1383. ISSN 1530-437X. DOI: 10.1109/JSEN.2011.2172602.
- [10] JIANG, G. L., H. YANG, R. LI and P. KONG. A new algorithm for a high-modulation frequency and high-speed digital lock-in amplifier. *Measurement Science and Technology*. 2015, vol. 27, iss. 1, pp. 1377–1383. ISSN 1361-6501. DOI: 10.1088/0957-0233/27/1/015701.
- [11] KHIARAK, M. N., B. GOSSELIN, S. MARTEL and Y. DE KONINCK. A CMOS lock-in-amplifier with semi-digital automatic phase tuning. In: *2016 IEEE Biomedical Circuits and Systems Conference (BioCAS)*. Shanghai: IEEE, 2016, pp. 300–303. ISBN 978-1-5090-2959-4. DOI: 10.1109/BioCAS.2016.7833791.
- [12] About Lock-In Amplifier. In: *thinkSRS* [online]. 2018. Available at: [http://physics.indiana.edu/~courses/p451/background\\_info/SRS\\_Lock-In\\_Amplifiers.pdf](http://physics.indiana.edu/~courses/p451/background_info/SRS_Lock-In_Amplifiers.pdf).
- [13] FAZEL, Z., S. SAEEDI and M. ATARODI. Pipelining method for low-power and high-speed SAR ADC design. *Analog Integrated Circuits and Signal Processing*. 2016, vol. 87, iss. 3, pp. 353–368. ISSN 0925-1030. DOI: 10.1007/s10470-016-0736-y.
- [14] MIRZAEI, A., H. DARABI, A. YAZDI, Z. ZHOU, E. CHANG and P. SURJ. A 65 nm CMOS Quad-Band Saw Less Receiver SoC for GSM/GPRS/EDGE. *IEEE Journal of Solid-State Circuits*. 2011, vol. 46, iss. 4, pp. 950–964. ISSN 1558-173X. DOI: 10.1109/JSSC.2011.2109570.
- [15] SHOKREKHODAEI, M., A. SAFARIAN and M. ATARODI. Transmitter leakage cancellation technique for CMOS SAW-less radio front-ends. *Analog Integrated Circuits and Signal Processing*. 2017, vol. 93, iss. 3, pp. 383–394. ISSN 1573-1979. DOI: 10.1007/s10470-017-1054-8.
- [16] DARABI, H. *Radio Frequency Integrated Circuits and Systems*. 1st ed. Cambridge: Cambridge University Press, 2015. ISBN 978-0-521-19079-4.
- [17] ARSALAN, F., S. USTABAS and H. ARSALAN. An Amperometric Biosensor for Glucose Determination Prepared from Glucose Oxidase Immobilized in Polyaniline-Polyvinylsulfonate Film. *Analog Sensors*. 2011, vol. 11, iss. 8, pp. 8152–8163. ISSN 1424-8220. DOI: 10.3390/s110808152.
- [18] LEE, W.-C., C.-C. KUO and N.-F. CHIU. Simple fabrication of glucose biosensor based on Graphene-Nafion composite by amperometric detections. In: *2012 IEEE Sensors*. Taipei: IEEE, 2012, pp. 1–4. ISBN 978-1-4577-1767-3. DOI: 10.1109/ICSENS.2012.6411155.
- [19] PARK, J.-H., C.-S. KIM, B.-C. CHOI and K.-Y. HAM. The correlation of the complex dielectric constant and blood glucose at low frequency. *Biosensors and Bioelectronics*. 2003, vol. 19, iss. 4, pp. 321–324. ISSN 0956-5663. DOI: 10.1016/S0956-5663(03)00188-X.
- [20] HEINEMANN, L., U. KRAMER, H.-M. KLOTZER, M. HEIN, D. VOLZ, M. HERMANN, T. HEISE and K. RAVE. Noninvasive Glucose Measurement by Monitoring of Scattering Coefficient During Oral Glucose Tolerance Tests. *Diabetes Technology & Therapeutics*. 2000, vol. 2, iss. 2, pp. 211–220. ISSN 1520-9156. DOI: 10.1089/15209150050025168.
- [21] RAHMAT, M. A., E. L. M. SU, M. MOHD ADDI and C. F. YEONG. GluQo: IoT-Based Non-invasive Blood Glucose Monitoring. *Journal of Telecommunication Electronic and Computer Engineering (JTEC)*. 2017, vol. 9, no. 3–9, pp. 71–75. ISSN 2289-8131.

## About Authors

**Maryamsadat SHOKREKHODAEI** was born in Isfahan, Iran. She received the M.Sc. degree (with honors) from Sharif University of Technology, Tehran, Iran. She is now working towards the Ph.D. degree in University of Texas at El Paso (UTEP), Texas, USA. Her main research interests are integrated bioelectronics, RF/analog ICs, and biomedical circuits/systems design.

**Stella QUINONES** was born in El Paso, TX, USA, Country. She received her M.Sc. degree in Metallurgical and Materials Engineering and her Ph.D. in Materials Science and Engineering from The University of Texas at El Paso (UTEP). She has been an Associate Professor in the Electrical and Computer Engineering department at UTEP since 2004. Her research interests include non-invasive biomedical sensors, 3D printing, and Engineering Education.

**Ziba FAZEL** was born in Urmia, Iran. She received the M.S. degree in electronics engineering from Sharif University of Technology (SUT), Tehran, Iran. She is currently pursuing her Ph.D. in electronic engineering at SUT. Her main research interests include RF/analog/mixed-signal integrated systems and circuits design for low power wireless communications and electronic interfaces of different daily life applications.

**Homer NAZERAN** holds B.Sc., M.Sc. and Ph.D. degrees in Electrical (Honors), Clinical and Biomedical Engineering from UT Austin, Case Western Reserve and University of Texas Southwestern Medical Center (UTSWM) at Dallas/UTA, respectively. He has more

than 3 decades of experience in industry and academia and has practiced and taught biomedical engineering in the Middle East, Europe, Australia and USA. In Australia, he co-founded the School of Engineering at the Flinders University of South Australia, introduced and established the electrical and electronics and biomedical engineering degree programs (1991 to 2001). He returned to the University of Texas at Arlington as a visiting professor in 1997 and 2001. He joined UTEP in 2002 to create and establish biomedical engineering degree programs at the Department of Electrical and Computer Engineering. His research interests are in the areas of computer modeling of physiological systems, intelligent biomedical instrumentation and biomedical signal processing as applied to chronic health conditions and telemedicine. He has more than 200 journal and conference articles in his research areas published in IEEE Engineering in Medicine and Biology Society (EMBS) and other flagship international conference proceedings. He is a reviewer for several national and international journals in his related fields including IEEE Transactions on Biomedical Engineering, Medical and Biological Engineering and Computing, Biomedical Engineering Online and others. His teaching interests are in electronics, biomedical instrumentation, physiological systems, and biomedical signal processing. He is also interested in development of novel teaching methods, lifelong learning and critical thinking habits in the classroom and interdisciplinary education based on application of nonlinear dynamics systems (complexity) theory. Professor Nazeran is the proud recipient of the UT Regent's Outstanding Teaching Award in 2015. His research, teaching and professional activities have been supported by NIH, NSF, and DOE among others.